5-2005

Cancer Promoted by the Oncoprotein v-ErbA May Be Due to Subcellular Mislocalization of Nuclear Receptors

Ghislain M.C. Bonamy

Anne Guiochon-Mantel

Lizabeth A. Allison

0888-8809/05/$15.00/0
Printed in U.S.A.

Molecular Endocrinology 19(5):1213–1230

doi: 10.1210/me.2004-0204

Cancer Promoted by the Oncoprotein v-ErbA May Be Due to Subcellular Mislocalization of Nuclear Receptors

Ghislain M. C. Bonamy, Anne Guiochon-Mantel, and Lizabeth A. Allison

The College of William and Mary (G.M.C.B., L.A.A.), Department of Biology, Williamsburg, Virginia 23187; Institut National de la Santé et de la Recherche Médicale (INSERM) Unité 693-Récepteurs Stéroïdiens, Physiopathologie endocrinienne et métabolique (G.M.C.B., A.G.M.), Faculté de Médecine Paris Sud, 94276 Le Kremlin-Bicetre Cedex France; and Université Paris 7-Denis-Diderot (G.M.C.B.), 75251 Paris Cedex 05, France

The retroviral v-ErbA oncoprotein is a highly mutated variant of the thyroid hormone receptor α (TRα), which is unable to bind T_3 and interferes with the action of TRα in mammalian and avian cancer cells. v-ErbA dominant-negative activity is attributed to competition with TRα for T_3-responsive DNA elements and/or auxiliary factors involved in the transcriptional regulation of T_3-responsive genes. However, competition models do not address the altered subcellular localization of v-ErbA and its possible implications in oncogenesis. Here, we report that v-ErbA dimerizes with TRα and the retinoid X receptor and sequesters a significant fraction of the two nuclear receptors in the cytoplasm. Recruitment of TRα to the cytoplasm by v-ErbA can be partially reversed in the presence of ligand and when chromatin is disrupted by the histone deacetylase inhibitor trichostatin A. These results define a new mode of action of v-ErbA and illustrate the importance of cellular compartmentalization in transcriptional regulation and oncogenesis. (*Molecular Endocrinology* 19: 1213–1230, 2005)

THE THYROID HORMONE receptor α (TRα) regulates gene activity through alternatively silencing or activating transcription in response to T_3. Most members of the nuclear receptor superfamily require ligand binding for functional activity. TR is unusual in that it is bound to target genes both in the presence and absence of ligand. Depending on the DNA response element to which the receptor is bound, TRα acts as a repressor (or activator in some cases) of specific genes in the absence of T_3 and as an activator (or repressor) of these same genes in the presence of T_3. By mediating T_3 action, TRα exerts important functions in homeostasis and development. Interest in TRα-regulated developmental pathways was enhanced by the discovery of the viral oncogene v-*erb*A carried by the avian erythroblastosis virus (AEV) (1). AEV induces fatal erythroleukemia dependent on the activity of two oncogenes v-*erb*A and v-*erb*B. Both v-*erb*A and v-*erb*B interfere with normal cell regulatory pathways to promote proliferation rather than differentiation. v-ErbB, a mutant form of the epidermal growth factor receptor, promotes cell proliferation, whereas v-ErbA, a mutant form of TRα that does not bind T_3, inhibits differentiation of erythroblast progenitors by quenching the expression of erythroid-specific genes (2, 3).

In mammalian and avian cancer cells, v-ErbA contributes to tumor formation in part by interfering with the action of liganded and unliganded TRα (4–7). The exact mechanism for transcriptional repression by v-ErbA has not yet been determined; however, two complementary models for the dominant-negative action of v-ErbA are well supported in the literature (8). In the first model, competition for DNA binding accounts for the dominant-negative activity: the oncoprotein binds to a thyroid hormone-responsive element (TRE) and blocks the recruitment of TRα to its TRE (9, 10). In the second model, dominant-negative activity is attributed to competition for TRα auxiliary factors and cofactors such as the retinoid X receptor β (RXRβ) (11–13). In both models, v-ErbA interferes with TRα and subverts regulation of T_3-responsive genes.

Interested in understanding the molecular basis behind the oncogenic conversion of TRα into v-ErbA, and the mode of action of dominant-negative transcription factors in general, we studied a relatively unexplored mode of oncogenic action: the effect of altered subcellular localization. TRα has a predominantly nuclear distribution at steady state but shuttles

First Published Online January 13, 2005

Abbreviations: AEV, Avian erythroblastosis virus; Ar, Ex argon laser; CFP, cyan fluorescent protein; CRM1, chromosome region maintenance 1; DCLP, Dichroic Long Pass; DsRed, red fluorescent protein; ER, endoplasmic reticulum; FRET, fluorescence resonance energy transfer; GFP, green fluorescent protein; GST, glutathione-*S*-transferase; HA, hemagglutinin; LMB, leptomycin B; 1p and 2p, one- and two-photon excitation; pbFRET, photobleaching of the acceptor; RA, retinoic acid; RXR, retinoid X receptor; TRα, thyroid hormone receptor α; TRE, thyroid hormone-responsive element; TSA, trichostatin A; YFP, yellow fluorescent protein.

***Molecular Endocrinology* is published monthly by The Endocrine Society (http://www.endo-society.org), the foremost professional society serving the endocrine community.**

rapidly between the nuclear and cytoplasmic compartments, providing an additional checkpoint in the control of T_3-responsive gene expression (14). In contrast, the oncoprotein v-ErbA exhibits a nucleocytoplasmic distribution pattern distinct from TRα. Both cytoplasmic and nuclear populations of v-ErbA are present at steady state in transfected mammalian cells (14, 15) and in avian cells infected with AEV (16). According to the current models of dominant-negative activity of v-ErbA described above, the oncoprotein must enter and be retained in the nucleus to interfere with the action of both liganded and unliganded TRα (4, 7, 17–21). However, this is inconsistent with the observation that much of v-ErbA remains cytoplasmic (14, 15).

Here we report that v-ErbA dimerizes with both TRα and RXRβ and sequesters a significant fraction of these two members of the nuclear receptor superfamily in the cytoplasm. Recruitment of TRα to the cytoplasm by v-ErbA can be partially reversed in the presence of ligand and when chromatin is disrupted by the histone deacetylase inhibitor trichostatin A (TSA). These results define a new mode of action of v-ErbA and illustrate the importance of cellular compartmentalization in transcriptional regulation and oncogenesis.

RESULTS

The Oncoprotein v-ErbA Mislocalizes TRα to the Cytoplasm

The oncoprotein v-ErbA differs from its cellular homolog, TRα, by fusion at its C terminus with a retroviral Gag sequence and by several amino acid substitutions, along with deletions at both the C and N termini (Fig. 1A). These sequence alterations have resulted in a loss of hormone binding and transactivation activity, altered DNA binding specificity, and a nucleocytoplasmic distribution distinct from TRα. At steady state, the majority of TRα is found in the nucleus in a diffuse pattern in transfected mammalian cells (14, 15). This pattern is identical for untagged and epitope-tagged counterparts. In contrast, v-ErbA has both cytoplasmic and nuclear populations at steady state, with distributions ranging from diffuse localization in both compartments to a primarily cytoplasmic distribution with distinct punctate foci (14, 15).

To investigate the important question of whether alterations in subcellular localization also play a role in oncogenesis, the effect of v-ErbA on the distribution of TRα was assessed after coexpression in mammalian cells, by a combined approach of epifluorescence and laser scanning confocal microscopy. Strikingly, when v-ErbA was coexpressed transiently, a subpopulation of TRα was also typically found in the cytoplasm of NIH/3T3 (mouse) cells with a punctate distribution pattern (Fig. 1B). Mislocalization of TRα was observed with every combination of fluorescent protein or epitope tag we tested, including green, yellow, cyan, and red fluorescent protein (GFP, YFP, CFP, and DsRed, respectively) and influenza A virus hemagglutinin (HA)-tagged v-ErbA (Fig. 1C).

Fluorescent proteins can form dimers or oligomers in some cases (22). Therefore, to ensure that the altered distribution pattern of TRα was not an artifact caused by interaction of the tags used, we also analyzed the distribution of GFP-TRα in the presence of untagged v-ErbA (Fig. 2A). Untagged v-ErbA had the same dramatic effect on TRα localization as its tagged counterparts. In the presence of untagged v-ErbA, GFP-TRα was mislocalized to cytoplasmic foci. Untagged v-ErbA has a distribution pattern comparable to fluorescent protein and epitope-tagged v-ErbA. Indirect immunofluorescence assays using anti-c-ErbA-specific antibodies revealed a distribution pattern ranging from a diffuse nuclear and cytoplasmic localization to cytoplasmic foci (Fig. 2B). When we increased the ratio between the amount of untagged v-ErbA and GFP-TRα expression vector used for the cotransfections, in a dose-response experiment, there was a positive correlation between the relative increase in untagged v-ErbA and the amount of TRα recruited to the cytoplasm. When cells were transfected with a 19-fold excess of untagged v-ErbA expression plasmid, no cells displayed a primarily nuclear distribution of TRα. In contrast, about 43% of the cells exhibited a primarily nuclear distribution when they were transfected with a 19-fold excess of GFP-TRα expression plasmid (Fig. 2C).

NIH/3T3 cells have been shown previously to be a suitable model for studies addressing the transcriptional activity and nucleocytoplasmic shuttling of TR and variants (14, 15). To ensure that the cytoplasmic mislocalization of TRα by v-ErbA was not a property of NIH/3T3 cells only, we also studied the interaction of coexpressed TRα and v-ErbA in HeLa (human) cells and COS-1 (African green monkey) cells. Both HeLa and COS-1 cells have been used extensively in studies addressing the dominant-negative properties of v-ErbA and the transcriptional activity of TR and RXR (13, 23–29). A distribution pattern similar to that of NIH/3T3 cells was also observed in HeLa and COS-1 cells (data not shown), confirming that NIH/3T3 cells are a representative model system.

Taken together, our findings show that the oncoprotein v-ErbA mislocalizes TRα to the cytoplasm in a dose-dependent manner. Importantly, this mislocalization is neither cell type specific nor is it caused by nonspecific interaction between fluorescent protein tags.

Recruitment of TRα to the Cytoplasm by v-ErbA Can Be Partially Reversed in Presence of Ligand

To determine whether liganded or unliganded TRα was more sensitive to cytoplasmic mislocalization by v-ErbA, the effect of T_3 on subcellular distribution at steady state (4–6 h incubation) was assessed. When v-ErbA was coexpressed with TRα in the absence of T_3, the distribution of TRα shifted significantly ($P < 0.0001$) from 95 $\pm$ 6% of cells with a nuclear distribu-

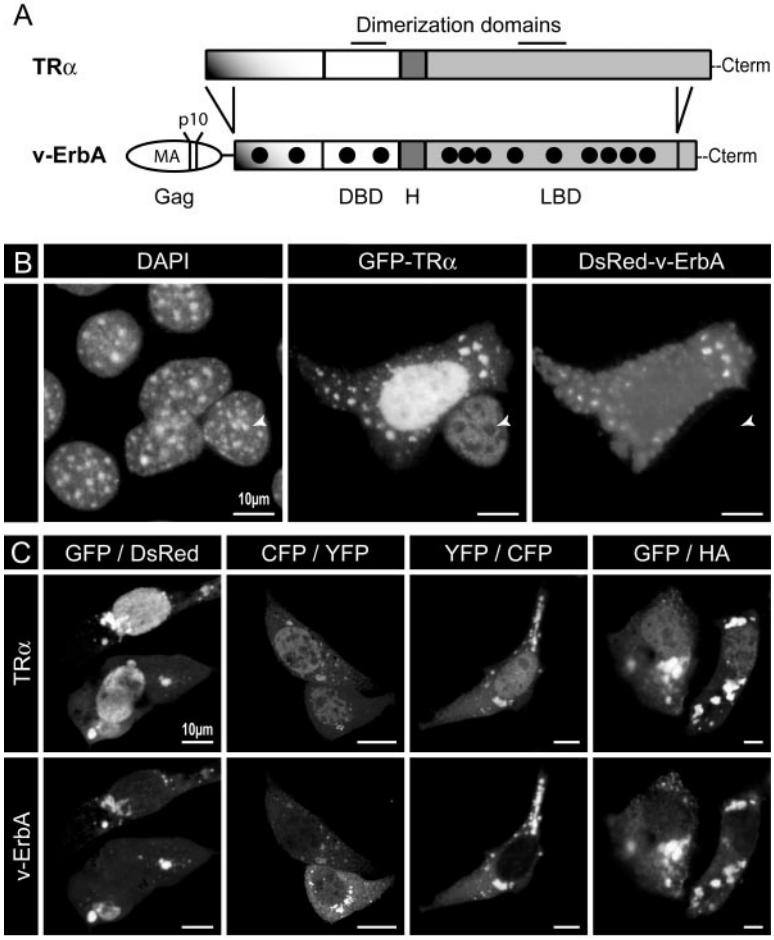

Fig. 1. TRα Is Mislocalized to the Cytoplasm in the Presence of v-ErbA

A, Schematic diagram (not to scale) of the oncoprotein v-ErbA illustrating its homology with TRα. v-ErbA differs from TRα by fusion at its C terminus (Cterm) with a retroviral Gag sequence and by several amino acid substitutions (*black circles*), along with deletions at both the C and N termini. MA, Matrix association domain, p10: domain containing the CRM1-dependent nuclear export sequence; LBD, ligand binding domain; DBD, DNA binding domain; DAPI, 4′,6-Diamidino-2-phenylindole. The *two horizontal bars* indicate the known dimerization domains of TRα. B, NIH/3T3 cells were cotransfected with vectors encoding GFP-TRα and DsRed-v-ErbA. Cells were observed by epifluorescence microscopy, after staining with the DNA stain DAPI to reveal the nucleus. When coexpressed with DsRed-v-ErbA, a significant fraction of GFP-TRα was found in the cytoplasm. In a cell not expressing DsRed-v-ErbA (*white arrowheads*), TRα was predominantly nuclear. C, Cells were transfected with TRα and v-ErbA fused to various epitope and fluorescent protein tags (GFP-TRα/DsRed-v-ErbA, CFP-TRα/YFP-v-ErbA, YFP-TRα/CFP-v-ErbA, GFP-TRα/HA-v-ErbA) and the subcellular localization of TRα and v-ErbA was imaged by confocal microscopy. HA-v-ErbA was analyzed by indirect immunofluorescence using anti-HA-specific antibodies. Mislocalization of TRα to the cytoplasm was observed for all combinations of tags.

tion (all N or N >C) to only 64 ± 6% of cells with a nuclear distribution of TRα (Fig. 3). Incubating cells for greater than 6 h in ligand did not alter this steady-state distribution of TRα (data not shown).

In contrast to the distribution pattern in the absence of T_3, when ligand was present, a significantly greater ($P < 0.001$) amount of TRα localized to the cell nucleus instead of being sequestered by v-ErbA in the cytoplasm (Fig. 3D). Addition of T_3 resulted in 85 ± 5% of the cells having a more nuclear localization of TRα (all N or N >C) compared with 64 ± 6% in the absence of ligand (Fig. 3D), even though neither the subcellular distribution of TRα nor v-ErbA alone is sensitive to T_3 (14) (Fig. 3, B and C). These results suggest that v-ErbA may function as a dominant-negative repressor of TRα action, in part, by sequestering wild-type TRα in abnormal cellular compartments, and that unliganded TRα is more sensitive to mislocalization.

v-ErbA Also Mislocalizes RXRβ, an Auxiliary Factor for TRα, to the Cytoplasm

TRα functions in regulating T_3-dependent gene expression as a heterodimer with RXR (23). In addition, RXR has been shown to form heterodimers with v-ErbA *in vitro* (11–13, 20, 30, 31). To determine whether an additional mode of action of v-ErbA involves sequestering this important auxiliary factor for TRα in the

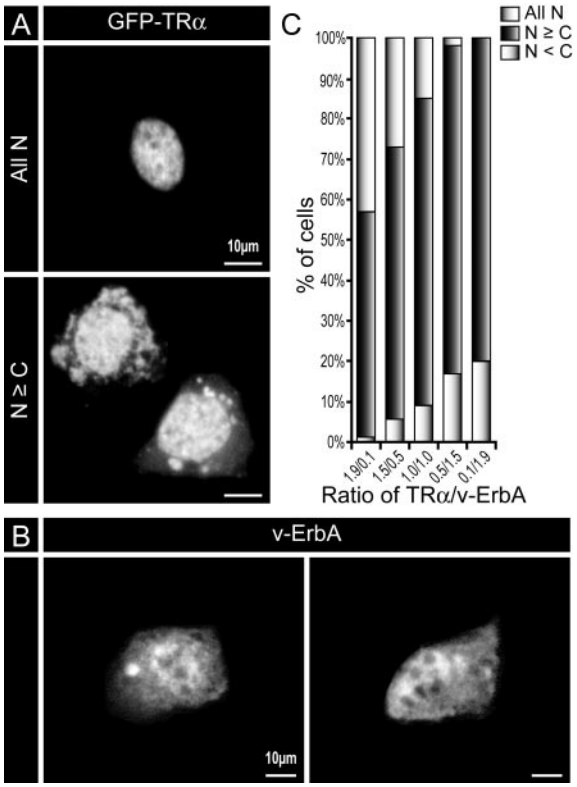

Fig. 2. Nuclear Localization of TRα Decreases in the Presence of Increasing Amounts of Untagged v-ErbA

A, Representative example of the distribution of GFP-TRα in the absence of v-ErbA (All N) and in cells transfected with a 0.5/1.5 ratio of TRα/v-ErbA expression vector (N $\geq$ C). B, Representative examples of untagged v-ErbA detected by indirect immunofluorescence. C, Cells were cotransfected with varying ratios of untagged v-ErbA and GFP-TRα expression vectors for a total of 2 μg of DNA, as indicated. The subcellular distribution of GFP-TRα was analyzed by epifluorescence microscopy. Cells were analyzed for nucleocytoplasmic distribution according to three categories: all N, completely nuclear; N $\geq$ C, mainly nuclear or whole cell; N $<$ C, mainly cytoplasmic. The sample size (number of cells scored) was 100 for all treatments.

cytoplasm, we assessed the effect of v-ErbA on the subcellular distribution of RXRβ. At steady state, the majority of RXRβ is found in the cell nucleus in a diffuse pattern (32) (Fig. 4A). Here, we show that in cells coexpressing GFP-RXRβ and HA-v-ErbA, a subpopulation of RXRβ is found in the cytoplasm in a punctate distribution pattern, similar to the pattern seen for TRα (Fig. 4A). This cytoplasmic mislocalization was also observed using other tag combinations such as GFP/DsRed, CFP/YFP and YFP/CFP (data not shown; see Figs. 5–6 for CFP/YFP), indicating that the altered distribution pattern of RXRβ is not due to interaction between the protein tags themselves. Interestingly, the action of v-ErbA is not limited to genes regulated by TR. It has been shown previously that the oncoprotein interferes with the transcription of other genes, including those regulated by RXR (13, 33, 34) and the retinoic acid (RA) receptor (30, 33). Thus, our observation that v-ErbA also mislocalizes RXR is consistent with the wider action of v-ErbA on genes regulated by other nuclear receptors.

TRα and RXRβ Colocalize with v-ErbA in the Cytoplasm

Having shown that the presence of v-ErbA dramatically alters the subcellular distribution of TRα and RXRβ, we sought to ascertain whether this change in distribution pattern was due to dimerization of the oncoprotein with these receptors. To this end, mammalian cells cotransfected with GFP-TRα or GFP-RXRβ and DsRed-v-ErbA were scored, without prior knowledge of the treatment, for colocalization of the two proteins according to three categories (Fig. 4B). Approximately 93 $\pm$ 10% of the v-ErbA-expressing cells displayed either total or partial colocalization of TRα with the oncoprotein in the absence of T_3 (Fig. 4C). Similarly, 94 $\pm$ 3% of the cells displayed either total or partial colocalization of RXRβ with v-ErbA (Fig. 4D). This colocalization was particularly evident in overlapping cytoplasmic punctate signals (Fig. 4, A and B; see also Fig. 1, B and C).

To determine whether increasing the level of oncoprotein expressed would strengthen the degree of colocalization with TRα, a dose response assay was performed. When the ratio between the amount of v-ErbA and TRα expression vector used for transfections was varied, there was a positive correlation between the relative increase in v-ErbA and an increase in TRα colocalization with v-ErbA in the cytoplasm (Table 1). Up to 94% of cells showed colocalization (partial or total) at a 19-fold excess of v-ErbA expression plasmid, increasing from 45% colocalization when there was a 19-fold excess of TRα expression plasmid.

Previous studies have reported that T_3 disrupts TR/TR homodimers and favors the formation of TR/RXR heterodimers (35). However, *in vitro* v-ErbA/TRα heterodimers remain bound to TREs at a physiological concentration of T_3 (100 nM) (8). To determine whether T_3, which restores TRα to the nucleus, also disrupts interaction of TR and v-ErbA *in vivo*, the effect of T_3 on colocalization was assessed. Restoration of TRα to the nucleus in the presence of T_3 was concomitant with a significant decrease in cytoplasmic colocalization with v-ErbA ($P < 0.0001$) (Fig. 4C). In the presence of ligand, the percentage of cells with no or partial colocalization of TRα and v-ErbA increased to 65 $\pm$ 7%, compared with 39 $\pm$ 7% in the absence of ligand. These results suggest that ligand-bound TRα is more resistant to the formation of inactive heterodimers with v-ErbA and may preferentially form transcriptionally active heterodimers with RXR.

These observations correlate with our previous observation that T_3, which normally has no effect on TRα localization, reduces the amount of the receptor in the cytoplasm when it is coexpressed with v-ErbA. This

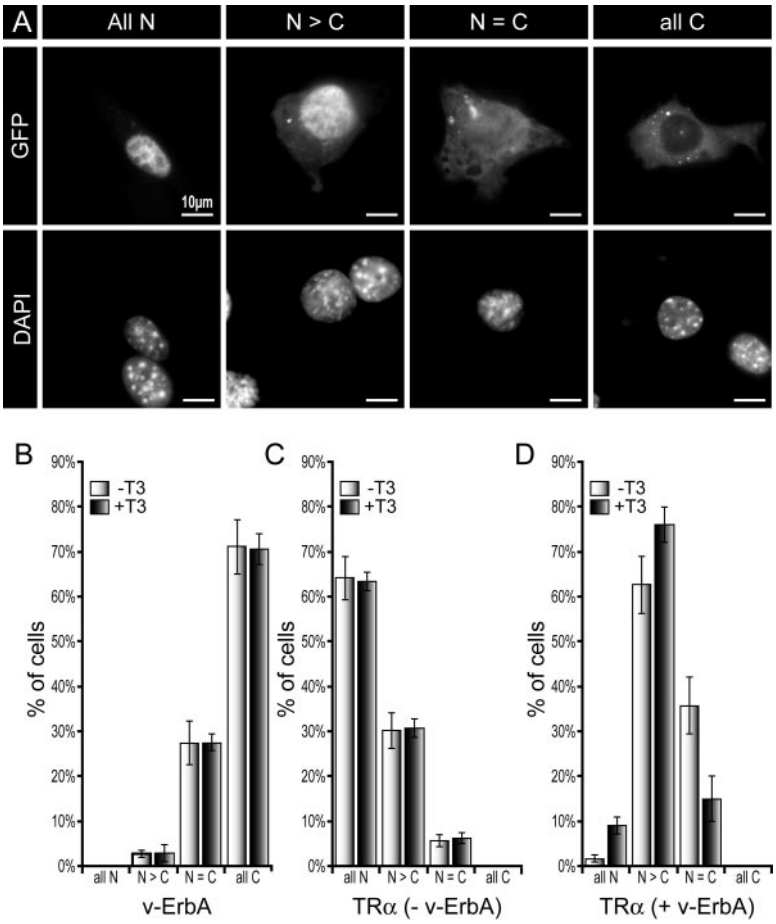

Fig. 3. Recruitment of TRα to the Cytoplasm by v-ErbA Can be Partially Reversed in the Presence of T_3

A, Categories of nucleocytoplasmic distribution: all N, completely nuclear; N >C, mainly nuclear; N = C, whole cell; all C, mainly to entirely cytoplasmic. These categories were used to score the variation in subcellular distribution of GFP-tagged proteins upon various treatments and to plot (B–D). The images depict cells transfected with a GFP-TRα expression vector and analyzed by epifluorescence microscopy after staining with DAPI to reveal the nucleus. B–D, Bar graphs summarizing the effect of 100 nM T_3 on the distribution of DsRed-v-ErbA (B) and GFP-TRα (C) expressed separately and together (D). GFP-TRα distribution was scored blind (without prior knowledge of the treatment) according to the categories in (A).

model is also consistent with previous reports which showed that addition of T_3 causes a slight increase in the transcription of genes normally repressed by the oncoprotein and inhibits proliferation of v-ErbA-transformed erythroblasts (6). Furthermore, as we expected, the presence of T_3 had no significant effect on the colocalization of RXRβ with v-ErbA because neither protein binds this ligand (Fig. 4D). However, unexpectedly, there was no significant ($P = 0.10$) change in RXR/v-ErbA colocalization in the presence of 9-*cis* RA (data not shown). Our findings are consistent with reports that T_3 causes a conformational change in TRα that alters its dimerization affinity (35) and, more specifically in this case, its affinity for v-ErbA.

v-ErbA Does Not Colocalize TRα to any of the Major Organelles Studied

The colocalization of TRα or RXRβ with v-ErbA in cytoplasmic foci was confirmed using confocal microscopy. Visual colocalization was not due merely to occasional, random overlapping of TRα or RXRβ with v-ErbA (Fig. 5A). Foci comprised of both TRα or RXRβ and v-ErbA have a similar pattern to cytoplasmic foci present in cells solely transfected with v-ErbA. The punctate patterns containing both v-ErbA and TRα or RXRβ were mainly oval shaped (Fig. 5A) but did not always have the same appearance in every case.

Whether the punctate cytoplasmic distribution of v-ErbA represents localization to specific cytoplasmic subcompartments was investigated by using a panel of compartment-specific probes. To determine whether the punctate cytoplasmic foci represent delivery of misfolded v-ErbA to lysosomes or endosomes for degradation, we examined the colocalization of GFP or YFP-tagged v-ErbA with Lysotracker Red or with the endosome-targeting construct CFP-Endo, respectively. v-ErbA often shows perinuclear and punctate staining, characteristic of

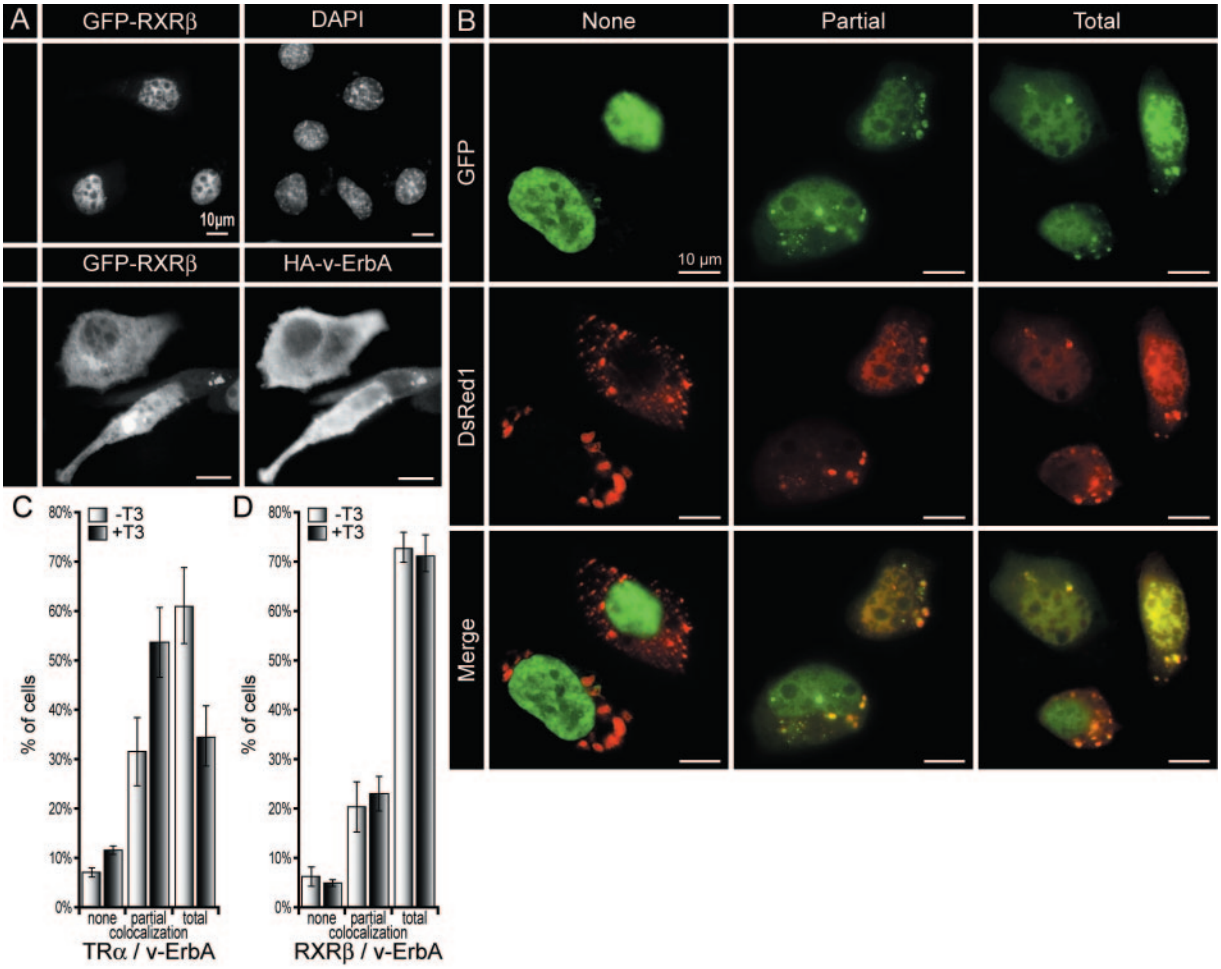

Fig. 4. TRα and RXRβ Colocalize with v-ErbA

A, Cells in the *upper panels* were transfected with an expression vector for GFP-RXRβ alone and the nuclei were stained with DAPI. In the *bottom panels* cells were cotransfected with both expression vectors for GFP-RXRβ and HA-v-ErbA. The subcellular distribution of GFP-RXRβ was observed by direct epifluorescence microscopy and HA-v-ErbA was detected by indirect immunofluorescence assay using anti-HA-specific antibodies. B, Categories of colocalization: none, partial, and total. These categories were used to score the variation in subcellular colocalization of GFP or YFP-tagged proteins with DsRed or CFP-tagged proteins upon various treatments and to plot (C) and (D). These images depict cells cotransfected with GFP-TRα and DsRed-v-ErbA expression vectors and analyzed by epifluorescence microscopy. The colocalization categories chosen were identical for GFP-RXRβ and DsRed-v-ErbA. C–D, Bar graphs summarizing the effect of 100 nM T_3 on colocalization with v-ErbA. Cells were scored blind (without knowledge of treatment) for colocalization according to the categories in (B). Cells were cotransfected with TRα and v-ErbA (C), or RXRβ and v-ErbA (D).

the Golgi and the endoplasmic reticulum (ER). To investigate whether or not the oncoprotein colocalizes with these organelles, we analyzed the distribution pattern of YFP-v-ErbA with ER-Tracker Blue-White and the Golgi-specific marker CFP-Golgi. Finally, given that a TR-like protein has been found to be associated with rat liver mitochondria (36), we also tested for aberrant mitochondrial localization of v-ErbA by staining GFP-v-ErbA transfected cells with Mitotracker Red. v-ErbA cytoplasmic foci showed no colocalization with any of these compartment-specific probes (Fig. 5B; and data not shown). There was occasional overlapping of v-ErbA foci with an organelle marker, but the spatial distributions overall were not positively correlated. Thus, the punctate distribution of the oncoprotein does not represent localization to lysosomes, endosomes, Golgi, endoplasmic reticulum, or mitochondria.

To determine whether cytoplasmic foci containing both TRα and v-ErbA localized to different cellular subcompartments than foci of v-ErbA alone, we tested for colocalization of v-ErbA/TRα with endosomes and Golgi. No colocalization of YFP-TRα coexpressed with DsRed-v-ErbA was observed with the CFP-Endo or CFP-Golgi probes (Fig. 5C). This indicates that TRα and v-ErbA are not localized to

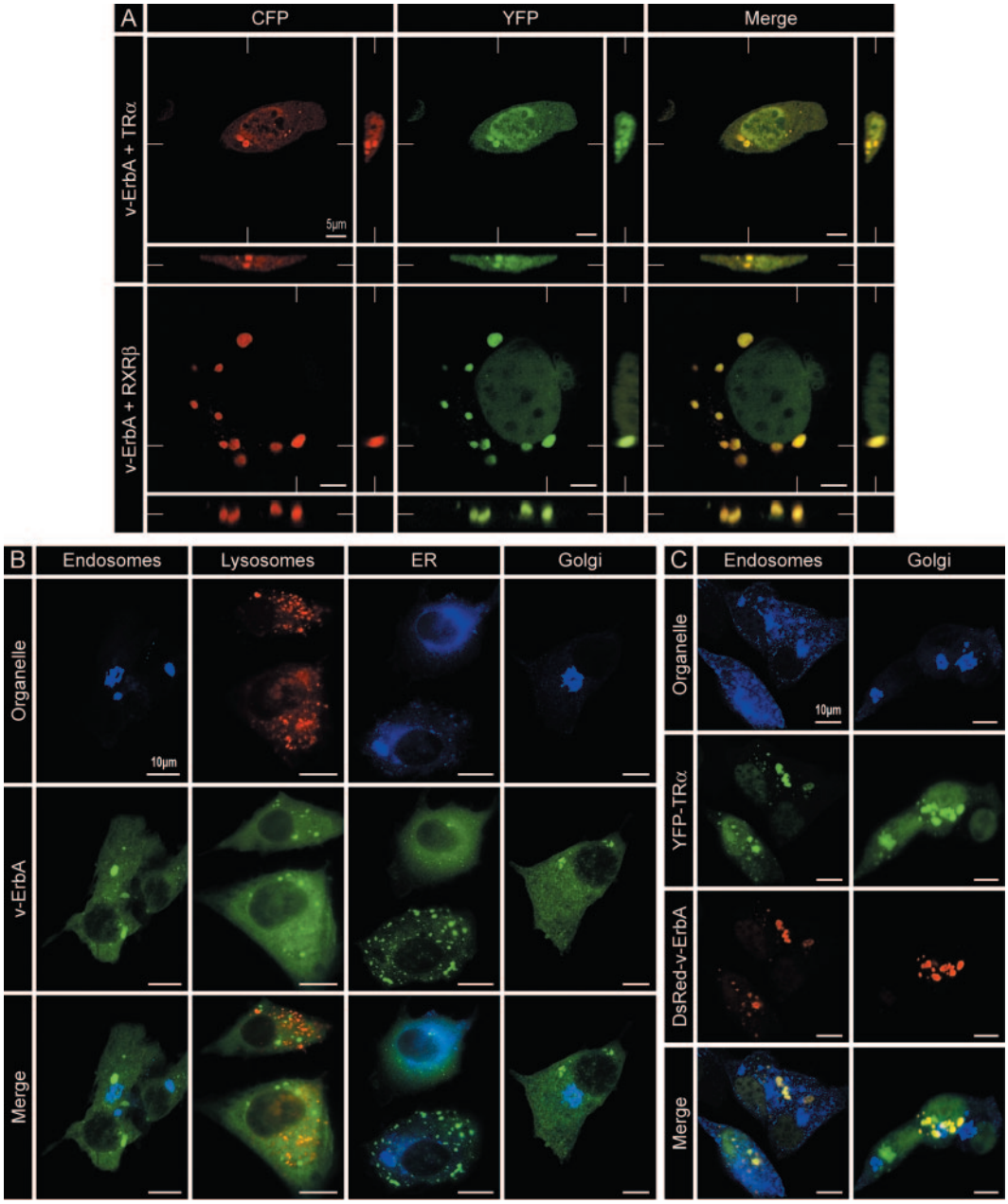

Fig. 5. v-ErbA Cytoplasmic Foci Colocalize with TRα and RXRβ but not with Various Organelles

A, Confocal images of cells coexpressing CFP-v-ErbA (*red*) and YFP-TRα (*green*) or CFP-v-ErbA (*red*) and YFP-RXRβ (*green*) are shown. Marks along each longitudinal section correspond to the position of reconstituted cross-sections (pictures to the *right* and *bottom* of the main panel). This three-dimensional reconstruction of the transfected cells reveals that the TR/v-ErbA foci are ovoid and vesicular-like structures, but not more complex networks. B, Cells transfected with GFP or YFP-tagged v-ErbA (*green*) were stained with ER Tracker Blue-White (*blue*) or Lysotracker Red (*red*) or cotransfected with expression vectors for CFP-Endo (endosomes), or CFP-Golgi (*blue*) and analyzed for colocalization by epifluorescence microscopy. Merged images revealed no colocalization between v-ErbA and the organelles studied. C, Cells cotransfected with YFP-TRα (*green*), and DsRed-v-ErbA (*red*) and with CFP-Endo (endosomes) or CFP-Golgi (*blue*), were analyzed for colocalization. Merged images show strong colocalization between TR and v-ErbA, but none with the organelle probes. The images of cells expressing CFP-Endo and CFP-Golgi in (B) and (C) were collected by confocal microscopy and represent the stacked projection of a Z-series.

the endosomes or trapped in the Golgi apparatus. More importantly, these findings provide further evidence that the colocalization observed between TRα and v-ErbA is not an artifact caused by interaction of the fluorescent protein tags. In addition, foci were never observed in cells transfected solely with expression vectors for unfused GFP, YFP, CFP, or DsRed (data not shown).

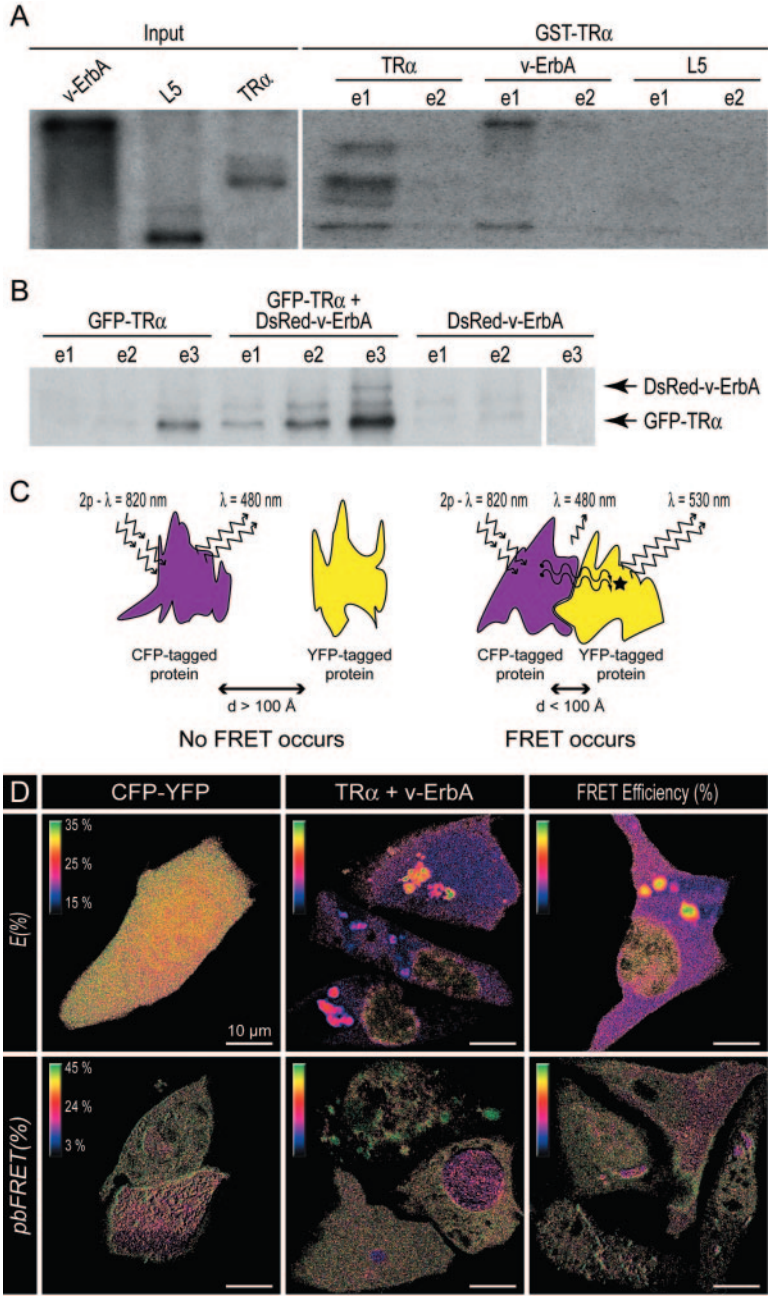

Fig. 6. TRα and v-ErbA Interact *in Vitro* and *in Situ*

A, GST pull-down assays were performed using GST-TRα and ^{35}S-labeled TRα, v-ErbA, or ribosomal protein L5 as a negative control. Input and binding fractions (elutions e1 and e2) are shown. Proteins were detected by fluorography. v-ErbA is eluted after binding to GST-TRα. B, TRα and v-ErbA interact *in situ*. COS-1 cells were cotransfected with vectors encoding GFP-TRα and/or DsRed-v-ErbA, and proteins were metabolically labeled with ^{35}S-methionine. Cell extracts were subject to coimmunoprecipitation assays using anti-GFP antibodies. e1, e2, and e3, Elutions of immunoprecipitates. Eluted ^{35}S-labeled proteins were detected by fluorography. The identity of radiolabeled protein bands was confirmed by comparing with known size standards and by Western blot analysis with anti-GFP and anti-DsRed-specific antibodies (data not shown). DsRed-v-ErbA is immunoprecipitated by anti-GFP antibodies via interaction with GFP-TRα. C, Schematic explanation of FRET principle. FRET occurs between CFP and YFP-tagged proteins only when they are within 100 Å from one another. When FRET occurs, the donor (CFP) emission is quenched, whereas the acceptor (YFP) emission is sensitized. D, Representative examples of FRET collected using the sensitized emission of the acceptor [*E(%)*] or using photobleaching of the acceptor [*pbFRET(%)*] in fixed NIH/3T3 cells transfected with the CFP-YFP fusion protein construct or cotransfected with equal amounts of expression vectors for CFP-v-ErbA and either YFP-TRα or YFP-RXRβ. *Calibration bar*: Intensity represents the efficiency of FRET *E(%)* or *pbFRET(%)* in percentage. Note the higher within sample variability for pbFRET compared with sensitized emission of the acceptor. In some cytoplasmic foci and in some nuclei the efficiency of FRET between CFP-v-ErbA and YFP-TRα or YFP-RXRβ was comparable to that of the positive control, CFP-YFP (*left panels*). The FRET signal recorded was significantly higher than the negative control (CFP+ YFP, data not shown).

Table 1. Colocalization of TRα with v-ErbA in the Presence of Increasing Amounts of v-ErbA

	Ratio of TRα/v-ErbA				
	1.9/0.1	1.5/0.5	1.0/1.0	0.5/1.5	0.1/1.9
% Colocalized	45	74	83	93	94
Sample size	40	42	47	46	18

Cells were cotransfected with varying ratios of GFP-TRα and DsRed-v-ErbA expression vectors for a total of 2 μg of DNA, as indicated, and analyzed for colocalization as described in Fig. 4. % Colocalized, Cells with partial or total colocalization of TRα and v-ErbA. The sample size corresponds to the number of cells scored.

Histone Deacetylation Enhances the Effect of Ligand on the Disruption of TRα and v-ErbA Colocalization

Transcriptional activation by liganded TR requires histone acetylation and remodeling of chromatin (37, 38). To determine whether hyperacetylation of histones would enhance nuclear retention of T_3-bound TRα, cells coexpressing TRα and v-ErbA were treated with TSA, a histone deacetylase inhibitor (39). In the presence of TSA, the percentage of cells exhibiting partial or total cytoplasmic colocalization of TRα and v-ErbA decreased from 73% to 56%. Concomitant with this disruption of colocalization, the percentage of cells showing primarily nuclear localization of TRα increased from 27% to 44%. Interestingly, there was a striking additive effect of T_3 and TSA on the disruption of TRα and v-ErbA colocalization (Table 2). Together, T_3 and TSA reduced the percentage of cells exhibiting partial or total colocalization to only 24% (Table 2). Associated with this disruption of colocalization, the percentage of cells showing primarily nuclear localization of TRα increased to 76%. Not surprisingly, when cells expressing GFP-TRα alone were treated with T_3 and/or TSA the distribution of the nuclear receptor remained unchanged (Fig. 3C; and data not shown). The sequestration of normal TRα in abnormal cellular compartments is thus partially reversed in the presence of hyperacetylated, active chromatin.

Table 2. Additive Effect of T_3 and TSA on the Nuclear Localization of TR and Disruption of TR and v-ErbA Colocalization

	Treatment			
	$-$TSA/$-T_3$	$+$TSA/$-T_3$	$-$TSA/$+T_3$	$+$TSA/$+T_3$
% All nuclear	27	44	62	76
% Colocalized	73	56	38	24
Sample size	250	250	250	250

Cells were cotransfected with expression vectors for GFP-TRα and DsRed-v-ErbA and treated with 100 nM T_3 and/or 100 nM TSA, as indicated. Nuclear localization and colocalization were analyzed as described in Figs. 3 and 4, respectively. % All nuclear, Subpopulation of cells coexpressing v-ErbA in which TRα was primarily localized in the nucleus. % Colocalized, Subpopulation of cells with either partial or total colocalization of TRα and v-ErbA. The sample size corresponds to the number of cells scored.

In Vitro and *in Situ* Interaction of TRα and v-ErbA

Our data demonstrate that v-ErbA is able to partially retain TRα in the cytoplasm, suggesting that v-ErbA binds to TRα *in vivo*. Prior studies have only analyzed the interaction of v-ErbA and TRα in the context of their binding to DNA recognition sites as monomers, homodimers, or heterodimers (8, 40), although the direct interaction of v-ErbA and RXR in the absence of DNA has previously been shown using *in vitro* assays (11). To demonstrate a similar interaction between v-ErbA and TRα in the absence of DNA, glutathione-S-transferase (GST) pull-down, coimmunoprecipitation, and fluorescence resonance energy transfer (FRET) assays were performed. Consistent with the colocalization studies, *in vitro*-translated v-ErbA can physically interact with GST-TRα in the absence of DNA (Fig. 6A), and DsRed-v-ErbA is immunoprecipitated from cells cotransfected with GFP-TRα, using anti-GFP antibodies (Fig. 6B). Moreover, the close proximity between the oncoprotein and either TRα or RXRβ was observed *in situ* using FRET.

FRET microscopy detects the result of a nonradiative transfer of energy from a donor fluorophore to a nearby acceptor that can only occur over a distance less than about 100 Å (Fig. 6C) (41–45). When FRET occurs between a pair of fluorophores, the donor's emission signal is quenched, whereas a sensitized light is emitted by the acceptor above the spectral background signal. In the present study, CFP and YFP were used, respectively, as the donor and acceptor pair for FRET. To record FRET, there are a number of well-established approaches (46). Among these techniques, FRET can be recorded through the sensitization of the donor or through the dequenching of the donor after photobleaching of the acceptor (pbFRET). Traditionally, these approaches have used one-photon (1p) excitation (41, 43, 44, 47–50). More recently, however, two-photon (2p) excitation has become the method of choice for some applications (45, 51–53). Here, we assessed FRET via 2p sensitization of YFP and confirmed it with 1p acceptor photobleaching.

To analyze FRET through sensitization of the donor, we first collected 12 images of unfused CFP or YFP alone under the same settings. These images were used to measure the coefficients of spectral cross talk from CFP or YFP in the FRET channel, and to correct the images of cells coexpressing both donor and acceptor. Although, the cross-section of YFP and CFP is broader for 2p excitation than for 1p (54) at 820 nm, the CFP/YFP cross-section ratio is approximately 40–50 (55). This is important because, in FRET imaging, the higher the CFP/YFP cross-section ratio is at the wavelength used to image CFP, the smaller will be the YFP signal monitored in the FRET channel (less

cross talk). We found that 2p excitation for CFP/YFP FRET has similar cross talk compared with 1p (data not shown). Nevertheless, it is important to keep in mind when using other fluorophores that the large cross-section of many fluorophores with 2p excitation may make this technique unsuitable for other FRET pairs traditionally used with 1p excitation. Thus, it is imperative to optimize the 2p excitation wavelength for each FRET pair used, especially to minimize the excitation of the donor when exciting the acceptor.

Second, 12 images of cells coexpressing both unfused CFP and YFP (CFP+YFP) together were collected as a negative control for FRET and 12 images of cells expressing the CFP-YFP fusion construct (44) were collected as a positive control for FRET. The positive control exhibits a 30% FRET efficiency (Fig. 6D). This value was used to quantify precisely the efficiency of FRET between TRα or RXRβ and v-ErbA. Finally, without prior knowledge of the treatment, we recorded images of cells displaying obvious colocalization of TRα or RXRβ with v-ErbA. At least 18 images each of cells coexpressing YFP-TRα or YFP-RXRβ with CFP-v-ErbA in the presence or absence of ligand were collected from three different transfection experiments. A significantly higher FRET signal ($P < 0.001$) was measured between both TRα+v-ErbA and RXRβ+v-ErbA compared with that of the negative control CFP+YFP. These data confirm that both RXR and TR colocalize with v-ErbA. On average, the FRET efficiency between TRα or RXRβ and v-ErbA was 19% (Fig. 6D). With the widely used orientation factor of 2/3 (45), we calculated a distance of approximately 67±2 Å between the fluorescent tags, which is well below the 100 Å limit for FRET detection (Fig. 6C). We did not do any direct measurements of the dipole orientation of the heterodimers, so this value is only an approximation. However, the distance measured is similar to that of other proteins interacting in complexes, such as the vacuolar H^+-ATPase-a (VHA-a) and vacuolar H^+-ATPase-c (VHA-c) subunits in the vacuolar H^+-ATPase complex in plants (50). Because the DNA binding domain of RXR alone is 38 × 74 × 25 Å (56), the relatively small distance measured between CFP and YFP provides further evidence that there is direct interaction of the receptors with the oncoprotein. In the presence of ligand (T_3 or 9-*cis* RA), the efficiency of FRET was slightly reduced between v-ErbA and TRα or RXRβ (Table 3); however, this decrease was not statistically significant ($P = 0.017$ and $P = 0.022$, respectively). Finally, FRET signals greater than the positive control CFP-YFP (>30%), sometimes occurred within cytoplasmic foci and/or nuclei of cells coexpressing v-ErbA and either TRα or RXRβ (Fig. 6D).

To provide additional evidence for interaction between v-ErbA and either TRα or RXRβ *in situ*, we assessed FRET via recovery of the donor's fluorescence after pbFRET. Using this technique, we confirmed that FRET occurred between YFP-TRα or YFP-RXRβ and CFP-v-ErbA (Fig. 6D). The FRET efficiencies obtained with pbFRET in the absence of T_3, compared with those obtained with sensitized FRET, were slightly higher between CFP-v-ErbA and YFP-TRα (24 ± 7%, average of n = 8 repeats) or YFP-RXRβ (29 ± 4%, n = 10) (compare with Table 3). However, the values were lower for the CFP-YFP-positive FRET control (26 ± 6%, n = 13) compared with the expected 30%. Direct comparison of the efficiencies is not possible because the within sample variability ranged from 12–19% for pbFRET compared with 2–5% with sensitized FRET (Fig. 6D). Low reproducibility and high variability of pbFRET data has been described in a previous study (43). Therefore, pbFRET cannot conclusively verify the accuracy of the cross-talk corrections used in sensitized FRET. More importantly, the values obtained with pbFRET confirm that FRET occurs between YFP-TRα or YFP-RXRβ and CFP-v-ErbA.

Taken together, these data provide further confirmation that TRα and RXRβ can physically interact with v-ErbA *in situ* and show that DNA binding is not required for heterodimer formation or stability.

v-ErbA/TRα Heterodimers Follow a Chromosome Region Maintenance 1 (CRM1)-Mediated Nuclear Export Pathway

Because TRα and v-ErbA are both shuttling proteins, the sequestration of TRα/v-ErbA heterodimers in the cytoplasm could be explained by at least two mechanisms. One possibility is that v-ErbA, being mostly a cytoplasmic protein, interacts with TRα during its nucleocytoplasmic shuttling. Heterodimers would then be sequestered in the cytoplasm because v-ErbA itself is retained in the cytoplasm. Alternatively, the two proteins could interact in the nucleus. Heterodimers would then be actively and rapidly exported to the

Table 3. Effect of Ligand on FRET between CFP-v-ErbA and YFP-TRα or YFP-RXRβ

YFP-TRα + CFP-v-ErbA		*t* Test	YFP-RXRβ + CFP-v-ErbA		*t* Test
$-T_3$	$+T_3$		−RA	+RA	
E (%) = 19.14 ± 2.17 n = 21	E (%) = 17.69 ± 2.04 n = 18	p = 0.017	E (%) = 19.71 ± 2.18 n = 21	E (%) = 18.29 ± 1.83 n = 18	p = 0.022

Cells were cotransfected with CFP-v-ErbA and either YFP-TRα or YFP-RXRβ, and incubated in the presence or absence of 100 nM T_3 or 9-*cis* RA, as indicated. E(%), FRET efficiency in percentage. n, Number of cells imaged. *t* Test, Critical value measured between treatments. The images for FRET quantifications were collected without prior knowledge of the treatment from three different transfection experiments for each treatment.

cytoplasm by a CRM1-mediated pathway, because v-ErbA exits the nucleus by such a pathway, in contrast to TRα (14, 15). We thus sought to ascertain whether coexpressing v-ErbA with TRα would confer to TRα the ability to follow a CRM1-mediated export pathway. To explore this model, we used heterokaryon assays (Fig. 7A) to determine whether TRα nuclear export becomes sensitive to leptomycin B (LMB) in the presence of v-ErbA. LMB is a specific inhibitor of CRM1-mediated export (39). Heterokaryons (or, in some cases, monokaryons where only one of the mouse nuclei of the fused cells was transfected) were left to shuttle for 6 h to ensure a sufficient time for TRα shuttling, which normally occurs within 1.5 h (14). In the presence of v-ErbA, TRα nuclear export exhibited sensitivity to LMB because there was no detectable shuttling even after 6 h (Fig. 7B). Under the same conditions (presence of LMB) and incubation time, but in the absence of v-ErbA, TRα was able to shuttle. In contrast v-ErbA remains trapped within the mouse nucleus in the presence of LMB (Fig. 7B). These findings, in conjunction with our findings that TRα forms dimers *in vivo* with v-ErbA, indicate that a CRM1-mediated export pathway is most likely followed by v-ErbA/TRα heterodimers (Fig. 7B). These observations also suggest that TRα may normally enter and exit the nucleus as a homodimer or heterodimer. Even if not all TRα becomes LMB sensitive by virtue of its interaction with the oncoprotein, its export kinetics or nuclear retention are clearly greatly altered in the presence of v-ErbA. Whether there is, in addition, active retention or anchoring of TRα in the cytoplasm by v-ErbA and other associated factors remains to be determined.

DISCUSSION

The studies described in this report demonstrate a previously uncharacterized mode of action for the oncoprotein v-ErbA, which may contribute significantly to its dominant-negative activity. In our model (Fig. 8), we propose that in addition to the well characterized

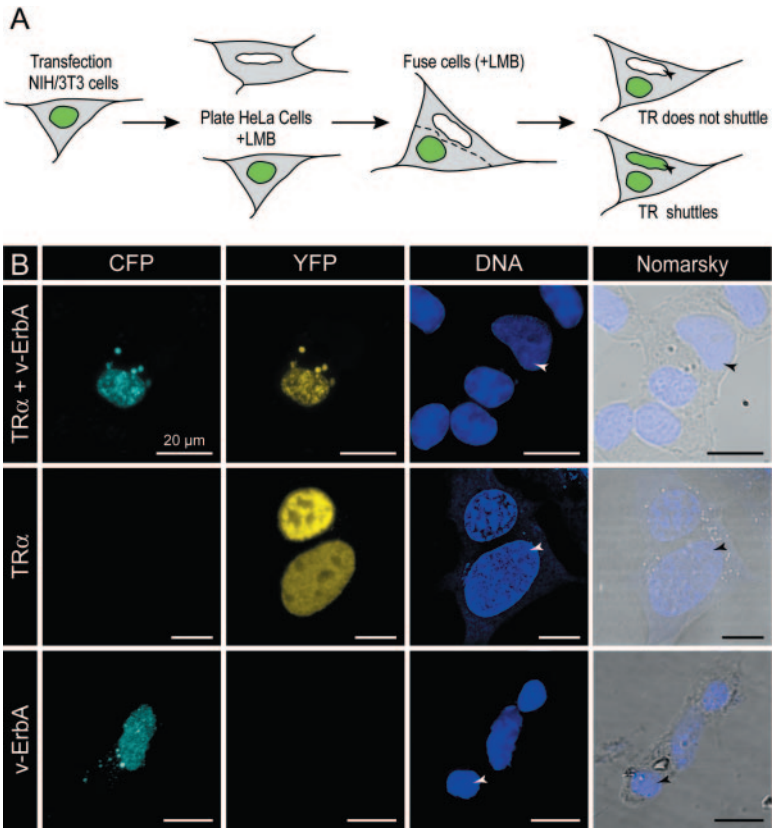

Fig. 7. v-ErbA/TRα Heterodimers Follow a CRM1-Mediated Nuclear Export Pathway

A, Schematic diagram of transient interspecies heterokaryon assay. B, Nucleocytoplasmic shuttling of YFP-TRα is blocked in the presence of CFP-v-ErbA and leptomycin B (LMB). NIH/3T3 cells were cotransfected with expression vectors for CFP-v-ErbA, YFP-TRα, or both. Subsequently, HeLa cells were fused with the transfected mouse cells to form heterokaryons, as confirmed by Nomarsky microscopy. The cells were incubated for 6 h in the presence of LMB. The *white arrowhead* points toward the human nucleus, as distinguished by differential staining with Hoechst and/or ToPro3, that should contain YFP-TRα or CFP-v-ErbA if shuttling occurs. v-ErbA nuclear export is blocked by the presence of LMB. Although TRα is able to shuttle in the presence of LMB alone, it is trapped in the nucleus in the presence of both v-ErbA and LMB.

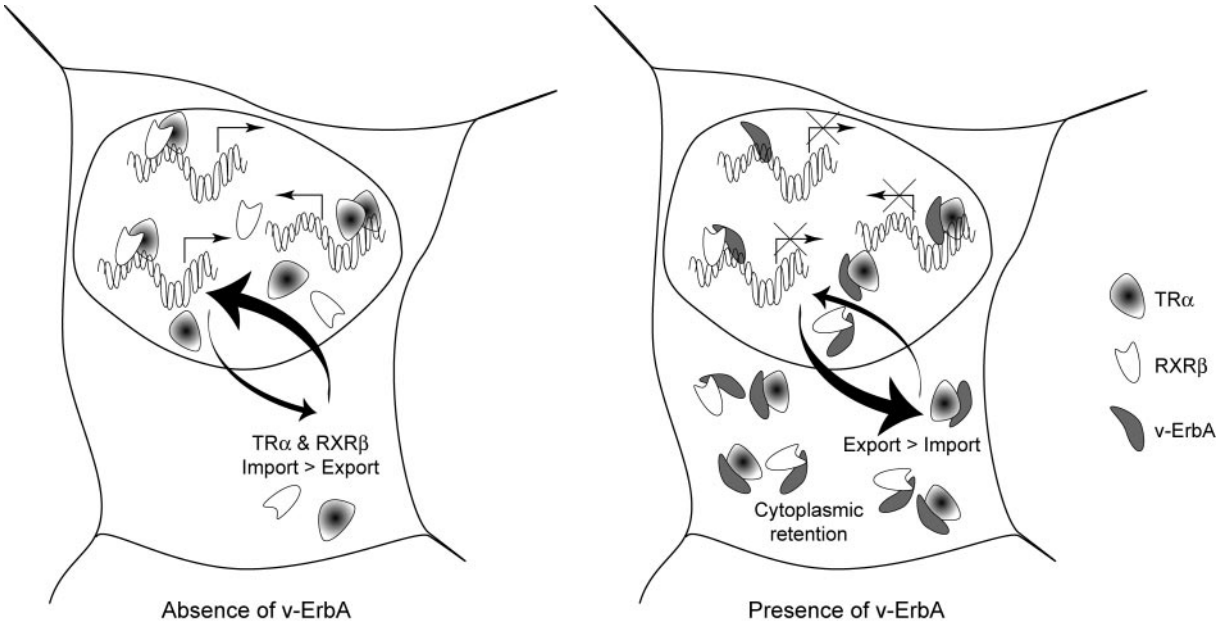

Fig. 8. Model of Dominant-Negative Activity of v-ErbA

In the absence of the oncoprotein, unliganded and liganded TRα along with RXRβ repress or enhance the transcription of specific genes. In the presence of v-ErbA, the normal transcriptional activity of TRα and RXRβ is antagonized by competition with v-ErbA for DNA response elements and/or cofactors, and mislocalization of TRα and RXRβ to the cytoplasm. Unliganded TRα is more sensitive to mislocalization; thus in the absence of ligand, cytoplasmic mislocalization may play a greater role in mediating v-ErbA dominant-negative activity. This mislocalization is most likely due to the active export by the CRM1-mediated export pathway of TRα/v-ErbA and RXRβ/v-ErbA heterodimers formed in the nucleus, and anchoring of these receptors by v-ErbA in the cytoplasm.

competition between v-ErbA and TR for TREs, the oncoprotein mediates the nuclear export of TR and its heterodimerization partner RXR. This CRM1-mediated export results in the sequestration of a subpopulation of both receptors in the cytoplasm. Such mislocalization provides a powerful level of repression by the oncoprotein, particularly for unliganded TR-mediated gene expression, leading to its oncogenic activity. When unliganded TR is mislocalized to the cytoplasm, it can no longer repress (or in some cases activate) expression of its target genes. In the presence of T_3, the dominant-negative activity of v-ErbA may be mediated to a greater degree by competition with TR for DNA-binding sites, in the nucleus. This model is supported by a previous study that showed that in the presence of T_3 v-ErbA dominant activity was reduced and transcriptional activity of two TR-responsive reporter constructs was partially restored (8). However, the incomplete restoration of TR to the nucleus, as well as the mislocalization of RXR and possibly other coactivators or corepressors of TR-mediated transcriptional regulation, suggest that cytoplasmic recruitment continues to play an important role even in the presence of T_3.

Earlier studies had suggested that v-ErbA acts by competing for DNA response elements rather than by formation of nonfunctional v-ErbA/TR heterodimers (9). These conclusions were based on transcription assays using a DNA binding domain mutant of v-ErbA; however, the subcellular localization of this mutant was not examined. Another DNA binding mutant of v-ErbA has been shown to be defective in its ability to accumulate in the nucleus (16, 57), illustrating the importance of DNA binding in nuclear import and retention. Our findings suggest that heterodimer formation may occur primarily in the nucleus. Therefore, in light of the data presented here and the link between the DNA binding domain and subcellular localization, it is highly likely that the DNA binding domain mutant of v-ErbA used in prior studies (9) would not have had the opportunity to form a heterodimer with nuclear TR, because of being localized to the cytoplasm.

Evidence from other studies supports the role of altered nuclear export, and cytoplasmic and/or nuclear mislocalization in transcriptional deregulation and oncogenesis. For example, mislocalization of INI1/hSNF5, a component of the SWI/SNF chromatin remodeling complex, blocks its normal tumor suppression function (58), p53 is hyperactively exported from the nucleus in some transformed cells (59), and ectopic expression of the hepatitis B virus X protein sequesters CRM1 in the cytoplasm, suggesting that the inactivation of the CRM1-mediated pathway may be an early step during viral-mediated liver carcinogenesis (60). Moreover, a recent report suggests that the hepatitis C virus core protein modulates the retinoid signaling pathway by sequestering Sp110b, a corepressor of the RA receptor α, to the endoplasmic

reticulum (61). Finally, a mutant of the androgen receptor, which is aberrantly localized in nuclear foci and subsequently mislocalizes steroid receptor coactivator 1, has been linked to human prostate cancer (62). Oncogenic conversion of TRα into v-ErbA thus not only involves changes in DNA binding specificity and ligand binding properties, but also the acquisition of altered nuclear export capabilities and subcellular localization (Fig. 8).

Mutants of the Rous sarcoma virus Gag polypeptide, as well as defective endogenous retroviruses have been shown to localize to the secretory pathway in host cells (63). Here we show that the portion of Gag fused to the N terminus of v-ErbA does not target v-ErbA to either the ER or the Golgi apparatus. Interestingly, this sequence of v-ErbA encompasses the matrix domain of Rous sarcoma virus Gag (Fig. 1), known to be responsible for membrane targeting (53, 63) and which may also be responsible for the formation of cytoplasmic complexes. Other viral Gag proteins have been reported to interact with various structures in the cytoplasm. For example, the Mason-Pfizer monkey virus matrix association domain of Gag interacts with the dynein/dynactin molecular motor and targets Gag to the pericentriolar region of the cell (64, 65). We recently reported that the altered nuclear export properties of v-ErbA are mainly attributed to a CRM1-dependent nuclear export sequence in the C-terminal portion of the p10 domain of Gag (15). Whether interaction and colocalization of Gag with subcellular components contributes to formation of foci is under investigation. Although the Gag domain may play a role in the formation of these cytoplasmic foci, it is unlikely that Gag is the sole contributor to the punctate distribution. We have observed a similar distribution in a DNA binding mutant of TRα (14). Likewise, a TRα mutant in which the entire D domain is deleted was shown by immunostaining to localize to the cytoplasm, and then over time to become localized to the perinuclear region or in cytoplasmic patches at the border of the nuclei (66). These observations suggest that cytoplasmic localization of TRα mutants and v-ErbA may have more to do with decreased nuclear retention, or a shift in the balance of nuclear import *vs.* nuclear export, than with Gag-mediated targeting to subcellular compartments.

The nature of v-ErbA cytoplasmic foci remains to be determined, but results presented here suggest that v-ErbA is not associated with a single organelle or other subcellular compartment. Furthermore, it is unlikely that these foci represent nonspecific aggregation of misfolded proteins because other studies suggest that, in cells, protein aggregation is highly specific (67). Cytoplasmic foci were not simply the result of aggregation of the DsRed tag, because a similar pattern of distribution was observed with CFP, YFP, and HA-tagged receptors, and when cells were cotransfected with expression vectors for untagged, native v-ErbA. Furthermore, in the presence of LMB, v-ErbA foci disperse over time and v-ErbA becomes trapped in the nucleus with a diffuse distribution pattern (Allison, L., unpublished observations), suggesting that these foci represent dynamic structures. Finally, cytoplasmic foci were not observed in cells transfected with expression vectors for unfused GFP, YFP, CFP, or DsRed.

The acquired oncogenic characteristics of v-ErbA, including a viral NES, lead to sequestration of normal TRα and auxiliary factors in the cytoplasm. This mislocalization can be partially reversed in the presence of ligand and active, hyperacetylated chromatin. Our findings, along with previous reports (10, 37, 38), emphasize the importance of chromatin structure for TR binding and transcriptional regulation. Although previous reports showed that the ligand for RXR, 9-*cis* RA, disrupts RXR/v-ErbA dimers and, moreover, allows the recovery of RXR transcriptional activity (13), we did not record a significant effect of ligand on the cytoplasmic colocalization of RXR and v-ErbA. However, the modest decrease in FRET efficiency suggests that 9-*cis* RA may partially disrupt RXR/v-ErbA dimers. It has been shown that the responsiveness of RXR to its ligand is greatly increased by the presence of TR (68). Therefore, it is possible that disruption of colocalization between RXR and v-ErbA, and concomitant restoration of RXR to the nucleus may require other factors, such as TR.

Our data show that increasing the amount of v-ErbA relative to TRα increases the degree of receptor mislocalization and colocalization with the oncoprotein in the cytoplasm. In some instances, inappropriate cytoplasmic accumulation of nuclear proteins labeled with GFP has been reported. For example, overexpression of GFP-tagged SMN (survival of motor neuron proteins) leads to aberrant cytoplasmic accumulation of SMN-complex proteins and core snRNP proteins in transiently transfected cells (69). However, cytoplasmic localization of v-ErbA is not a result of overexpression or tagging with GFP because we observed cytoplasmic accumulation over a range of different expression levels, and whether v-ErbA was fluorescent protein tagged, epitope tagged, or untagged. Furthermore, v-ErbA is naturally overexpressed in cells infected with AEV, and this strong expression is essential in host cells to mediate transforming activity (5, 9, 13). This phenomenon was previously explained solely by the relatively poor interaction of v-ErbA with TREs. In the presence of T_3, increasing amounts of v-ErbA relative to TR are required to increase v-ErbA transcriptional repression (8). This is consistent with our finding that increasing the amount of v-ErbA relative to that of TR increased the degree of mislocalization of the receptor to the cytoplasm, and that this overexpression could partially compensate for the disrupting action of T_3 on TR/v-ErbA dimers. It now appears that natural overexpression of the oncoprotein is necessary, in part, to mediate all components of dominant-negative activity, including subcellular mislocalization of TRα and RXR.

In summary, our findings not only increase understanding of the normal cellular response to T_3 but also

provide important insight into the ontogeny of an oncogene and modulation of gene expression through both compartmentalization and dominant-negative transcription factors. Other dominant-negative variants of TRα may be involved in human cancer (70); thus, these findings may have implications for a mechanism for their action as well.

MATERIALS AND METHODS

Gene Constructs

Expression vectors for GFP-TRα, GFP-v-ErbA, untagged v-ErbA (RS-v-*erb*A) and for *in vitro* translation of TRα, v-ErbA, and ribosomal protein L5 were as previously described (14, 71). Expression vectors for DsRed, YFP, and CFP-tagged TRα and v-ErbA were constructed by subcloning into pDsRed2-C1, pEYFP-C1 and pECFP-C1 plasmids (CLONTECH Laboratories, Inc., Palo Alto, CA). HA-v-ErbA was subcloned into pCMV-HA (CLONTECH) by PCR amplification of v-*erb*A with an engineered *Bgl*II site at the 5′-end and the existing *Eco*RI site from GFP-v-ErbA. Expression vectors for GFP-RXRβ and a CFP-YFP fusion protein were gifts from Y. Katagiri (32) and J. Swanson (44), respectively. pGEX-2T-T3R used for bacterial overexpression of GST-TRα was a gift from M. Privalsky (72).

Transient Transfection Assays

Transient transfection assays and subsequent analysis of fixed NIH/3T3 cells by epifluorescence microscopy were performed as described (14). Sixteen to 24 h after transfection, cells were incubated for 4–14 h with T_3 and 9-*cis* RA-depleted medium or with medium supplemented with 100 nM T_3 and/or 100 nM TSA or 100 nM 9-*cis* RA (Sigma, St. Louis, MO). The subcellular localization of untagged v-ErbA and HA-v-ErbA was analyzed by indirect immunofluorescence using standard procedures (14). Cells where probed with anti-c-*erb*A antibodies (1:50, rabbit polyclonal to full-length chicken TRα, FL-408; Santa Cruz Biotechnology, Inc., Santa Cruz, CA) or anti-HA (1:200, rabbit polyclonal, S1827, CLONTECH) and labeled secondary antibodies (1:100 and 1:500 respectively, Vector Laboratories, Inc., Burlingame, CA). Confocal images were collected with Laser Sharp 2000 version 5.3 (Bio-Rad, Hercules, CA) using the Radiance 2001 (Bio-Rad) laser scanning system, mounted on an inverted microscope (Nikon Eclipse TE300, Nikon Inc., Melville, NY). The following filter combinations were used: GFP Ex Argon laser (Ar) 514 nm, Dichroic Long Pass (DCLP) 560, high quality filter (HQ) 515/30; DsRed Helium Neon laser 543 nm, DCLP 560, DCLP 650, HQ 600/50; CFP Ar 457 nm, DCLP 500, HQ 485/30; YFP Ar 514 nm, DCLP 500, DCLP 650, HQ 545/40; DsRed He/Ne 570 nm, DCLP 500, DCLP 560, LP 570.

Analysis of v-ErbA Association with Specific Organelles

To analyze the colocalization of v-ErbA with lysosomes or endosomes, cells transfected with GFP or YFP-tagged v-ErbA were stained for 30 min at 37 C with Lysotracker Red DND-99 (100 nM, Molecular Probes, Eugene, OR) or cotransfected with an endosome-targeting vector, pECFP-Endo (CLONTECH). For Golgi and ER colocalization, YFP or GFP-v-ErbA transfected cells were stained for 30 min at 37 C just before the fixation with ER-Tracker Blue-White DPX (500 nM, Molecular Probes), or were cotransfected with a Golgi-specific targeting vector, pECFP-Golgi (CLONTECH). For mitochondrial association, GFP-v-ErbA transfected cells were incubated for 30 min at 37 C with Mitotracker Red (50 nM, Molecular Probes) just before fixation.

Analysis of Nucleocytoplasmic Distribution and Colocalization

Transfection experiments were carried out at least three times for each treatment, with greater than 100 cells analyzed per trial. Scoring of cells was performed blindly, without prior knowledge of treatment. For analysis of nucleocytoplasmic distribution, cells were categorized into four groups based on rigorous criteria for the qualitative assessment of the subcellular distribution of TRα: all N, complete nuclear localization; N $>$ C, mainly nuclear; N $=$ C, whole cell distribution; or all C, mainly to entirely cytoplasmic. For analysis of colocalization, cells were categorized into three groups based on qualitative rigorous criteria for the assessment of the relative degree of colocalization of TRα or RXRβ with v-ErbA: total, partial, or no colocalization. Log-linear analysis was used to determine the statistical significance of differences in subcellular distribution and colocalization in the presence and absence of v-ErbA and ligand.

GST Pull-Down and Coimmunoprecipitation Assays

Direct interaction between TRα and v-ErbA was examined by GST pull-down assays. The GST-TRα fusion protein was expressed in *Escherichia coli* BL21-Codon Plus (DE3)-RIL cells (Stratagene, La Jolla, CA). After induction with 0.5 M isopropyl-β-D-thiogalactopyranoside at 30 C, bacterial cells were harvested and sonicated in B-PER Bacterial Protein Extraction Reagent (Pierce, Rockford, IL) supplemented with 500 μg/ml lysozyme. GST-TRα was purified using Glutathione Sepharose 4B resin (Amersham Pharmacia Biotech, Arlington Heights, IL) and eluted with reduced glutathione, followed by dialysis against PBS. Purified protein was bound to Immobilized Glutathione gel in Mini-Spin Columns (Pierce), according to the manufacturer's instructions. Radiolabeled TRα, v-ErbA, and ribosomal protein L5 were translated *in vitro* using the TNT-coupled transcription/translation system (Promega) in the presence of ^{35}S-methionine (Amersham) and SP6 or T_3 RNA polymerase. Pull-down assays were carried out using the Profound Pull-Down GST Assay Kit (Pierce), according to the manufacturer's instructions. Samples were analyzed by 10% SDS-PAGE and fluorography was performed as described (14).

For coimmunoprecipitation assays, COS-1 cells were cotransfected with GFP-TRα and DsRed-v-ErbA expression plasmids in 100-mm plates. Twenty hours after transfection, transfection medium was replaced with DMEM containing 10% fetal bovine serum minus methionine (Invitrogen Life Technologies, Carlsbad, CA), supplemented with 50 μCi/ml ^{35}S-methionine. Cells were lysed 48 h after transfection in M-PER Reagent (Pierce) and incubated with anti-GFP antibody (CLONTECH Living Colors full-length *A.v.* polyclonal) bound to AminoLink Plus Coupling Gel in Mini-Spin Columns (Pierce), according to the manufacturer's instructions. After elution, immunoprecipitated antigen samples were concentrated using PAGEprep Protein Clean-Up and Enrichment Kit (Pierce) and analyzed by 10% SDS-PAGE and fluorography. The identity of radiolabeled protein bands was confirmed by comparing with known size standards (Bio-Rad Kaleidoscope prestained protein molecular weight standards) and by Western blot analysis with anti-GFP and anti-DsRed-specific antibodies (CLONTECH Living Colors *A.v.* monoclonal #JL-8; CLONTECH Living Colors DsRed monoclonal).

FRET Analysis

NIH/3T3 cells were transfected with expression vectors for unfused CFP, unfused YFP or CFP-YFP fusion protein alone,

or cotransfected with equal quantities of expression plasmids for both unfused CFP and YFP, or either CFP-TRα or CFP-RXRβ and YFP-v-ErbA. Transfected cells were fixed as described above. To measure the efficiency of FRET analysis via sensitized emission of YFP, all images were collected with 2p excitation. In monolayer cells, 2p excitation is reported to yield a FRET signal that is less affected by donor concentration than in one photon confocal FRET microscopy (45). However, the photobleaching rate under 2p excitation is higher at the focal plane than in 1p microscopy (73–76). The use of fixed cells and identical settings, allowed scanning of each sample only once for each wavelength. This helped reduced 2p high-order photobleaching and associated drawbacks. Nevertheless, it is important when designing an experiment using this technique on samples other than fixed monolayer cells to keep in mind the higher photobleaching properties at the focal plane of 2p excitation. The 2p-excitation was achieved with a Ti/Si laser line (MaiTai, Spectra-Physics, Mountain View, CA), connected to a Radiance 2100 (Bio-Rad) confocal microscope, using the same settings for each image collected (gain, offset, zoom, laser power). The channels used to collect the pictures were as follows: donor (CFP), 2p-820 nm, HQ 485/30; FRET 2p-820 nm, DCLP 500, HQ 528/50; acceptor (YFP) 2p-920 nm, DCLP 500, HQ 528/50. To reduce potential photobleaching CFP and FRET channels were collected simultaneously. Using the setcol display feature, the background (*Bkg*) was set as pixels with an intensity of five or less. To quantify the data, a correction algorithm was used that allows a more precise and more quantitative approach to FRET (44, 45). The correction algorithm was applied using scripts written with scientific imaging software (Scanalytics, Fairfax, VA) according to the following formula:

$$\begin{cases} cF = \begin{cases} F^{d,a} - \sum_{i=0}^{n-1} (r_i^d \times D_i^{d,a} + r_i^a \times A_i^{d,a}) & \forall (D_i^{d,a} \text{ and } A_i^{d,a}) \in]Bkg..Sat[\\ 0 & else \end{cases} \\ r_i^d = \dfrac{F^d}{D_i^d} \text{ and } r_i^a = \dfrac{F^a}{A_i^a} \quad \Big| \quad \begin{array}{l} \forall (D_i^d \text{ and } A_i^a) \in]Bkg..Sat[\\ \forall\ i \in [0..n[\end{array} \end{cases}$$

where *cF* corresponds to the corrected FRET signal; *D*, *F*, and *A* represent the images collected under the donor, FRET, and acceptor channels respectively, in samples transfected by: d, donor; a, acceptor; or a,b, both donor and acceptor, respectively. The index *i* represents the given range of intensity, and *n* was set to 5 bit (=32), delimiting a 3-bit (=8) range of intensity (for example, $A_3^{a,b}$ represents all the pixels that have an intensity between 24 and 31, from an image of cells coexpressing the donor and acceptor that was collected under the acceptor channel). The background (*Bkg*) or saturated pixels (*Sat*) of these images were set to zero using masks before the analysis. The cross-talk coefficients r^d and r^a were calculated for each range of intensity, *i*, using 12 different sets of images each from cells expressing donor or acceptor alone from three different slides. These cells were chosen with various intensity levels so that the entire dynamic range could be covered for the correction. In this case, F^a and F^d represent the sets of pixels with the same coordinates as in A_i^a and D_i^d, respectively.

The efficiency of FRET was then calculated for each sample using the following formula:

$$E(\%) = 100 \times \left(1 - \frac{A^{d,a}}{A^{d,a} + \gamma \cdot cF^{d,a}}\right)$$

where *E(%)* is the percent efficiency of FRET. γ corresponds to the ratio of ξ/γ in Hoppe *et al.* (44) or to $(\Psi_{dd}/\Psi_{dd}) \times Q_d$ in Elanglovan *et al.* (45). The efficiency of FRET for the construct expressing a CFP-YFP fusion protein was determined to be approximately 30% at pH 8.5 *in vitro* (pH of the mounting media used) (44). γ Was thus calculated by averaging 12 different sets of images collected from three different slides of cells transfected by the CFP-YFP fusion construct, according to the following equation:

$$\gamma = \left(\frac{E(\%)^{CFP-YFP}}{100 - E(\%)^{CFP-YFP}} \times \left\langle \frac{A^{CFP-YFP}}{cF^{CFP-YFP}} \right\rangle \right)_{\substack{\forall cF_i \neq 0 \\ E(\%)^{CFP-YFP} = 30\%}}$$

$A^{CFP\text{-}YFP}$ is the intensity of CFP-YFP collected under the acceptor channel, and $cF^{CFP\text{-}YFP}$ the intensity of the corrected FRET for CFP-YFP. γ was estimated to be approximately 0.5.

To ensure that the signal measured was due to FRET, 12 images from cells transfected solely with unfused CFP and YFP were collected from three different slides. Finally, for cells expressing YFP-TRα or YFP-RXRβ cotransfected with CFP-v-ErbA in the presence or absence of T_3 or RA, respectively, the images were collected blind from a total of 12 slides (three slides per treatment) without knowledge of treatment. The cells chosen for analysis were solely cells with obvious colocalization of YFP-TRα or YFP-RXRβ with CFP-v-ErbA. Distance was calculated according to the following formula:

$$r_{(\text{Å})} = R_0 \times 6 \sqrt{\left(\frac{100}{E(\%)} - 1\right)}$$

where $r_{(\text{Å})}$ is the distance in Angstrom, R_0, is the Förster's distance calculated to be 52.76 for the CFP/YFP FRET pair (45). This value of R_0 assumes the widely used dipole orientation of 2/3 (45). *E(%)* is the FRET efficiency.

For pbFRET, the signal was determined using the following formula:

$$pbFRET\ (\%) = \begin{cases} 100 \times \left(1 - \dfrac{D^{d,a}}{D^d}\right) & \forall (D^{d,a} \text{ and } D^d) \in]Bkg..Sat[\\ 0 & else \end{cases}$$

where *pbFRET* (%) is the FRET efficiency, $D^{d,a}$ are images collected under the donor channel before photobleaching (where donor and acceptor are present) and D^d are images collected under the donor channel after photobleaching of the acceptor (only the donor remains present) (41–43). $D^{d,a}$, D^d were collected using the setcol display feature, so that the background (Bkg) was set as pixels with an intensity of 5 or less. These pictures were then corrected for background and saturation if applicable. The cells were photobleached for 1–10 consecutive scans (≈78–780 μs/pixels at a 0.1–0.2 μm/pixel resolution) using the 514-nm laser line (5 mW) of the argon laser set at 100%. Images were captured under the YFP filter set, before and after photobleaching to confirm the loss of fluorescence.

Heterokaryon Assays

Heterokaryon assays were performed as described (14). In brief, NIH/3T3 cells were transfected with YFP-TRα and/or CFP-v-ErbA. Twenty to 24 h after transfection, HeLa cells were trypsinized and plated at high density with transfected NIH/3T3 cells. Three to 4 h after seeding, HeLa cells were fused to the transfected NIH/3T3 cells with polyethylene glycol at 50% wt/vol in 75 mM HEPES (Roche, Indianapolis, IN). LMB and/or cycloheximide (Sigma) were added after transfection at a final concentration of 5 ng/ml for the LMB, and 50 μg/ml for the first 30 min then 100 μg/ml thereafter for the cycloheximide. The heterokaryons were left to shuttle 6–8 h. The integrity of the heterokaryons was confirmed using transmission microscopy, and shuttling was indicated by the presence of YFP-TRα in both the transfected NIH/3T3 and untransfected HeLa cell nuclei. For differential staining of nuclei, the coverslips were incubated in a 100-μl drop of Dulbecco's PBS containing 0.5 μmol of To-Pro3 and/or 10 μg/ml of Hoechst for 15 min in the dark, then rinsed three times with

Dulbecco's PBS for 5 min before being mounted in VectaShield.

Acknowledgments

We thank Y. Katagiri, M. Privalsky, and J. Swanson for the gifts of GFP-RXRβ, pGEX-2T-T3R, and CFP-YFP, respectively; R. Day and A. Perisamy for advice regarding FRET; K. Walseman for expert technical assistance; H. Luo for pilot studies on colocalization; B. Gwinn and A. Chen for pilot studies using compartment-specific probes; and M. Case for comments on the manuscript.

Received May 18, 2004. Accepted January 7, 2005.

Address all correspondence and requests for reprints to: Lizabeth A. Allison, Department of Biology, College of William and Mary, P.O. Box 8795, Millington Hall 116, Williamsburg, Virginia 23187-8795. E-mail: laalli@wm.edu.

This work is part of the Ph.D. dissertation research of G. Bonamy under the supervision of A. Guiochon-Mantel and L. Allison, and was sponsored by funding from the National Institutes of Health (DK058028-01A1) and the National Science Foundation (MCB0090923) (to L.A.A.).

REFERENCES

1. Beug H, Bauer A, Dolznig H, von Lindern M, Lobmayer L, Mellitzer G, Steinlein P, Wessely O, Mullner E 1996 Avian erythropoiesis and erythroleukemia: towards understanding the role of the biomolecules involved. Biochim Biophys Acta 1288:M35–M47
2. Zenke M, Munoz A, Sap J, Vennstrom B, Beug H 1990 v-erbA oncogene activation entails the loss of hormone-dependent regulator activity of c-erbA. Cell 61: 1035–1049
3. Woods CM, Boyer B, Vogt PK, Lazarides E 1986 Control of erythroid differentiation: asynchronous expression of the anion transporter and the peripheral components of the membrane skeleton in AEV- and S13-transformed cells. J Cell Biol 103:1789–1798
4. Braliou GG, Ciana P, Klaassen W, Gandrillon O, Stunnenberg HG 2001 The v-ErbA oncoprotein quenches the activity of an erythroid-specific enhancer. Oncogene 20: 775–787
5. Damm K, Thompson CC, Evans RM 1989 Protein encoded by v-erbA functions as a thyroid-hormone receptor antagonist. Nature 339:593–597
6. Bauer A, Mikulits W, Lagger G, Stengl G, Brosch G, Beug H 1998 The thyroid hormone receptor functions as a ligand-operated developmental switch between proliferation and differentiation of erythroid progenitors. EMBO J 17:4291–4303
7. Barlow C, Meister B, Lardelli M, Lendahl U, Vennstrom B 1994 Thyroid abnormalities and hepatocellular carcinoma in mice transgenic for v-erbA. EMBO J 13: 4241–4250
8. Yen PM, Ikeda M, Brubaker JH, Forgione M, Sugawara A, Chin WW 1994 Roles of v-erbA homodimers and heterodimers in mediating dominant negative activity by v-erbA. J Biol Chem 269:903–909
9. Selmi S, Samuels HH 1991 Thyroid hormone receptor/and v-erbA. A single amino acid difference in the C-terminal region influences dominant negative activity and receptor dimer formation. J Biol Chem 266:11589–11593
10. Ciana P, Braliou GG, Demay FG, von Lindern M, Barettino D, Beug H, Stunnenberg HG 1998 Leukemic transformation by the v-ErbA oncoprotein entails constitutive binding to and repression of an erythroid enhancer in vivo. EMBO J 17:7382–7394
11. Shen Q, Subauste JS 2000 Dimerization interfaces of v-erbA homodimers and heterodimers with retinoid X receptor α. J Biol Chem 275:41018–41027
12. Subauste JS, Koenig RJ 1998 Characterization of the DNA-binding and dominant negative activity of v-erbA homodimers. Mol Endocrinol 12:1380–1392
13. Wahlstrom GM, Vennstrom B 1998 Requirements for repression of retinoid X receptor by the oncoprotein $P75^{gag\text{-}v\text{-}erbA}$ and the thyroid hormone receptors. Mol Endocrinol 12:645–653
14. Bunn CF, Neidig JA, Freidinger KE, Stankiewicz TA, Weaver BS, McGrew J, Allison LA 2001 Nucleocytoplasmic shuttling of the thyroid hormone receptor α. Mol Endocrinol 15:512–533
15. DeLong LJ, Bonamy GM, Fink EN, Allison LA 2004 Nuclear export of the oncoprotein v-ErbA is mediated by acquisition of a viral nuclear export sequence. J Biol Chem 279:15356–15367
16. Boucher P, Koning A, Privalsky ML 1988 The avian erythroblastosis virus erbA oncogene encodes a DNA-binding protein exhibiting distinct nuclear and cytoplasmic subcellular localizations. J Virol 62:534–544
17. Mey A, Gandrillon O, McNagny KM, Clegg DO, Samarut J 2002 The v-erbA oncogene blocks expression of $\alpha 2/\beta 1$ integrin a normal inhibitor of erythroid progenitor proliferation. Oncogene 21:2864–2872
18. Schroeder C, Raynoschek C, Fuhrmann U, Damm K, Vennstrom B, Beug H 1990 The v-erb A oncogene causes repression of erythrocyte-specific genes and an immature, aberrant differentiation phenotype in normal erythroid progenitors. Oncogene 5:1445–1453
19. Stunnenberg HG, Garcia-Jimenez C, Betz JL 1999 Leukemia: the sophisticated subversion of hematopoiesis by nuclear receptor oncoproteins. Biochim Biophys Acta 1423:F15–F33
20. Yen PM, Chin WW 1994 Molecular mechanisms of dominant negative activity by nuclear hormone receptors. Mol Endocrinol 8:1450–1454
21. Zenke M, Kahn P, Disela C, Vennstrom B, Leutz A, Keegan K, Hayman MJ, Choi HR, Yew N, Engel JD, Beug H 1988 v-erbA specifically suppresses transcription of the avian erythrocyte anion transporter (band 3) gene. Cell 52:107–119
22. Zacharias DA 2002 Sticky caveats in an otherwise glowing report: oligomerizing fluorescent proteins and their use in cell biology. Sci STKE 2002:PE23
23. Li D, Li T, Wang F, Tian H, Samuels HH 2002 Functional evidence for retinoid X receptor (RXR) as a nonsilent partner in the thyroid hormone receptor/RXR heterodimer. Mol Cell Biol 22:5782–5792
24. Busch K, Martin B, Baniahmad A, Renkawitz R, Muller M 1997 At least three subdomains of v-erbA are involved in its silencing function. Mol Endocrinol 11:379–389
25. Sande S, Sharif M, Chen H, Privalsky M 1993 v-erbA acts on retinoic acid receptors in immature avian erythroid cells. J Virol 67:1067–1074
26. de Verneuil H, Metzger D 1990 The lack of transcriptional activation of the v-erbA oncogene is in part due to a mutation present in the DNA binding domain of the protein. Nucleic Acids Res 18:4489–4497
27. Qi JS, Desai-Yajnik V, Yuan Y, Samuels HH 1997 Constitutive activation of gene expression by thyroid hormone receptor results from reversal of p53-mediated repression. Mol Cell Biol 17:7195–7207
28. Saatcioglu F, Lopez G, West BL, Zandi E, Feng W, Lu H, Esmaili A, Apriletti JW, Kushner PJ, Baxter JD, Karin M 1997 Mutations in the conserved C-terminal sequence in thyroid hormone receptor dissociate hormone-dependent activation from interference with AP-1 activity. Mol Cell Biol 17:4687–4695

29. Bogazzi F, Hudson LD, Nikodem VM 1994 A novel heterodimerization partner for thyroid hormone receptor. Peroxisome proliferator-activated receptor. J Biol Chem 269:11683–11686
30. Barettino D, Bugge TH, Bartunek P, Vivanco Ruiz MD, Sonntag-Buck V, Beug H, Zenke M, Stunnenberg HG 1993 Unliganded T3R, but not its oncogenic variant, v-erbA, suppresses RAR-dependent transactivation by titrating out RXR. EMBO J 12:1343–1354
31. Hermann T, Hoffmann B, Piedrafita FJ, Zhang XK, Pfahl M 1993 V-erbA requires auxiliary proteins for dominant negative activity. Oncogene 8:55–65
32. Katagiri Y, Takeda K, Yu ZX, Ferrans VJ, Ozato K, Guroff G 2000 Modulation of retinoid signalling through NGF-induced nuclear export of NGFI-B. Nat Cell Biol 2:435–440
33. Chen HW, Privalsky ML 1993 The erbA oncogene represses the actions of both retinoid X and retinoid A receptors but does so by distinct mechanisms. Mol Cell Biol 13:5970–5980
34. Zubkova I, Subauste JS 2003 Sequences required for the transition from monomeric to homodimeric forms of thyroid hormone receptor α and v-erbA. Mol Cell Endocrinol 199:61–72
35. Collingwood TN, Butler A, Tone Y, Clifton-Bligh RJ, Parker MG, Chatterjee VK 1997 Thyroid hormone-mediated enhancement of heterodimer formation between thyroid hormone receptor β and retinoid X receptor. J Biol Chem 272:13060–13065
36. Wrutniak C, Cassar-Malek I, Marchal S, Rascle A, Heusser S, Keller JM, Flechon J, Dauca M, Samarut J, Ghysdael J 1995 A 43-kDa protein related to c-Erb A α 1 is located in the mitochondrial matrix of rat liver. J Biol Chem 270:16347–16354
37. Li Q, Sachs L, Shi YB, Wolffe AP 1999 Modification of chromatin structure by the thyroid hormone receptor. Trends Endocrinol Metab 10:157–164
38. Urnov FD, Wolffe AP 2001 An array of positioned nucleosomes potentiates thyroid hormone receptor action in vivo. J Biol Chem 276:19753–19761
39. Yoshida M, Horinouchi S 1999 Trichostatin and leptomycin. Inhibition of histone deacetylation and signal-dependent nuclear export. Ann NY Acad Sci 886:23–36
40. Hollenberg AN, Monden T, Wondisford FE 1995 Ligand-independent and -dependent functions of thyroid hormone receptor isoforms depend upon their distinct amino termini. J Biol Chem 270:14274–14280
41. Day RN, Voss TC, Enwright JF, Booker CF, Periasamy A, Schaufele F 2003 Imaging the localized protein interactions between Pit-1 and the CCAAT/enhancer binding protein α in the living pituitary cell nucleus. Mol Endocrinol 17:333–345
42. Xia Z, Liu Y 2001 Reliable and global measurement of fluorescence resonance energy transfer using fluorescence microscopes. Biophys J 81:2395–2402
43. Berney C, Danuser G 2003 FRET or no FRET: a quantitative comparison. Biophys J 84:3992–4010
44. Hoppe A, Christensen K, Swanson JA 2002 Fluorescence resonance energy transfer-based stoichiometry in living cells. Biophys J 83:3652–3664
45. Elangovan M, Wallrabe H, Chen Y, Day RN, Barroso M, Periasamy A 2003 Characterization of one- and two-photon excitation fluorescence resonance energy transfer microscopy. Methods 29:58–73
46. Jares-Erijman EA, Jovin TM 2003 FRET imaging. Nat Biotechnol 21:1387–1395
47. Day RN 1998 Visualization of Pit-1 transcription factor interactions in the living cell nucleus by fluorescence resonance energy transfer microscopy. Mol Endocrinol 12:1410–1419
48. Day RN, Periasamy A, Schaufele F 2001 Fluorescence resonance energy transfer microscopy of localized protein interactions in the living cell nucleus. Methods 25: 4–18
49. Tertoolen LG, Blanchetot C, Jiang G, Overvoorde J, Gadella Jr TW, Hunter T, den Hertog J 2001 Dimerization of receptor protein-tyrosine phosphatase α in living cells. BMC Cell Biol 2:8
50. Kluge C, Seidel T, Bolte S, Sharma SS, Hanitzsch M, Satiat-Jeunemaitre B, Ross J, Sauer M, Golldack D, Dietz KJ 2004 Subcellular distribution of the V-ATPase complex in plant cells, and in vivo localisation of the 100 kDa subunit VHA-a within the complex. BMC Cell Biol 5:29
51. Wallrabe H, Stanley M, Periasamy A, Barroso M 2003 One- and two-photon fluorescence resonance energy transfer microscopy to establish a clustered distribution of receptor-ligand complexes in endocytic membranes. J Biomed Opt 8:339–346
52. Xu MG, Crimeen B, Ludford-Menting MJ, Gan X, Russell SM, Gu M 2001 Three-dimensional localisation of fluorescence resonance energy transfer in living cells under two-photon excitation. Scanning 23:9–13
53. Larson DR, Ma YM, Vogt VM, Webb WW 2003 Direct measurement of Gag-Gag interaction during retrovirus assembly with FRET and fluorescence correlation spectroscopy. J Cell Biol 162:1233–1244
54. Lansford R, Bearman G, Fraser SE 2001 Resolution of multiple green fluorescent protein color variants and dyes using two-photon microscopy and imaging spectroscopy. J Biomed Opt 6:311–318
55. Rovnyak D, Filip C, Itin B, Stern AS, Wagner G, Griffin RG, Hoch JC 2003 Multiple-quantum magic-angle spinning spectroscopy using nonlinear sampling. J Magn Reson 161:43–55
56. Bourguet W, Ruff M, Chambon P, Gronemeyer H, Moras D 1995 Crystal structure of the ligand-binding domain of the human nuclear receptor RXR-α. Nature 375:377–382
57. Boucher P, Privalsky ML 1990 Mapping of functional domains within the v-erb A oncogene protein: the remnants of the hormone binding domain play multiple, vital roles in protein action. Oncogene 5:1303–1311
58. Craig E, Zhang ZK, Davies KP, Kalpana GV 2002 A masked NES in INI1/hSNF5 mediates hCRM1-dependent nuclear export: implications for tumorigenesis. EMBO J 21:31–42
59. Stommel JM, Marchenko ND, Jimenez GS, Moll UM, Hope TJ, Wahl GM 1999 A leucine-rich nuclear export signal in the p53 tetramerization domain: regulation of subcellular localization and p53 activity by NES masking. EMBO J 18:1660–1672
60. Forgues M, Marrogi AJ, Spillare EA, Wu CG, Yang Q, Yoshida M, Wang XW 2001 Interaction of the hepatitis B virus X protein with the Crm1-dependent nuclear export pathway. J Biol Chem 276:22797–22803
61. Watashi K, Hijikata M, Tagawa A, Doi T, Marusawa H, Shimotohno K 2003 Modulation of retinoid signaling by a cytoplasmic viral protein via sequestration of Sp110b, a potent transcriptional corepressor of retinoic acid receptor, from the nucleus. Mol Cell Biol 23:7498–7509
62. Nazareth LV, Stenoien DL, Bingman 3rd WE, James AJ, Wu C, Zhang Y, Edwards DP, Mancini M, Marcelli M, Lamb DJ, Weigel NL 1999 A C619Y mutation in the human androgen receptor causes inactivation and mislocalization of the receptor with concomitant sequestration of SRC-1 (steroid receptor coactivator 1). Mol Endocrinol 13:2065–2075
63. Scheifele LZ, Rhoads JD, Parent LJ 2003 Specificity of plasma membrane targeting by the rous sarcoma virus gag protein. J Virol 77:470–480
64. Sfakianos JN, Hunter E 2003 M-PMV capsid transport is mediated by Env/Gag interactions at the pericentriolar recycling endosome. Traffic 4:671–680
65. Sfakianos JN, Lacasse RA, Hunter E 2003 The M-PMV cytoplasmic targeting-retention signal directs nascent

Gag polypeptides to a pericentriolar region of the cell. Traffic 4:660–670
66. Lee Y, Mahdavi V 1993 The D domain of the thyroid hormone receptor alpha 1 specifies positive and negative transcriptional regulation functions. J Biol Chem 268: 2021–2028
67. Rajan RS, Illing ME, Bence NF, Kopito RR 2001 Specificity in intracellular protein aggregation and inclusion body formation. Proc Natl Acad Sci USA 98:13060–13065
68. Zhang XK, Hoffmann B, Tran PB, Graupner G, Pfahl M 1992 Retinoid X receptor is an auxiliary protein for thyroid hormone and retinoic acid receptors. Nature 355: 441–446
69. Sleeman JE, Trinkle-Mulcahy L, Prescott AR, Ogg SC, Lamond AI 2003 Cajal body proteins SMN and Coilin show differential dynamic behaviour in vivo. J Cell Sci 116:2039–2050
70. Gonzalez-Sancho JM, Garcia V, Bonilla F, Munoz A 2003 Thyroid hormone receptors/THR genes in human cancer. Cancer Lett 192:121–132
71. Nagl SB, Nelson CC, Romaniuk PJ, Allison LA 1995 Constitutive transactivation by the thyroid hormone receptor and a novel pattern of activity of its oncogenic homolog v-ErbA in Xenopus oocytes. Mol Endocrinol 9:1522–1532
72. Tzagarakis-Foster C, Privalsky ML 1998 Phosphorylation of thyroid hormone receptors by protein kinase A regulates DNA recognition by specific inhibition of receptor monomer binding. J Biol Chem 273:10926–10932
73. Chirico G, Cannone F, Baldini G, Diaspro A 2003 Two-photon thermal bleaching of single fluorescent molecules. Biophys J 84:588–598
74. Chen TS, Zeng SQ, Luo QM, Zhang ZH, Zhou W 2002 High-order photobleaching of green fluorescent protein inside live cells in two-photon excitation microscopy. Biochem Biophys Res Commun 291:1272–1275
75. Patterson GH, Piston DW 2000 Photobleaching in two-photon excitation microscopy. Biophys J 78:2159–2162
76. Drummond DR, Carter N, Cross RA 2002 Multiphoton versus confocal high resolution z-sectioning of enhanced green fluorescent microtubules: increased multiphoton photobleaching within the focal plane can be compensated using a Pockels cell and dual widefield detectors. J Microsc 206:161–169

Molecular Endocrinology **is published monthly by The Endocrine Society (http://www.endo-society.org), the foremost professional society serving the endocrine community.**